



Article

Cite this article: Greve R, Chambers C, Obase T, Saito F, Chan W-L, Abe-Ouchi A (2023). Future projections for the Antarctic ice sheet until the year 2300 with a climate-index method. *Journal of Glaciology* 69(278), 1569–1579. <https://doi.org/10.1017/jog.2023.41>

Received: 13 May 2022

Revised: 20 May 2023

Accepted: 28 May 2023

First published online: 11 July 2023

Keywords:

Antarctic glaciology; climate change; ice and climate; ice-sheet modelling

Corresponding author:

Ralf Greve;

Email: greve@lowtem.hokudai.ac.jp

Future projections for the Antarctic ice sheet until the year 2300 with a climate-index method

Ralf Greve^{1,2} , Christopher Chambers¹ , Takashi Obase³ , Fuyuki Saito⁴ ,
Wing-Le Chan^{3,4}  and Ayako Abe-Ouchi³ 

¹Institute of Low Temperature Science, Hokkaido University, Sapporo, Japan; ²Arctic Research Center, Hokkaido University, Sapporo, Japan; ³Atmosphere and Ocean Research Institute, University of Tokyo, Kashiwa, Japan and ⁴Japan Agency for Marine-Earth Science and Technology, Yokohama, Japan

Abstract

As part of the Coupled Model Intercomparison Project Phase 6 (CMIP6), the Ice Sheet Model Intercomparison Project for CMIP6 (ISMIP6) was devised to assess the likely sea-level-rise contribution from the Earth's ice sheets. Here, we construct an ensemble of climate forcings for Antarctica until the year 2300 based on original ISMIP6 forcings until 2100, combined with climate indices from simulations with the MIROC4m climate model until 2300. We then use these forcings to run simulations for the Antarctic ice sheet with the SICOPOLIS model. For the unabated warming pathway RCP8.5/SSP5-8.5, the ice sheet suffers a severe mass loss, amounting to ~ 1.5 m SLE (sea-level equivalent) for the fourteen-experiment mean, and ~ 3.3 m SLE for the most sensitive experiment. Most of this loss originates from West Antarctica. For the reduced emissions pathway RCP2.6/SSP1-2.6, the loss is limited to a three-experiment mean of ~ 0.16 m SLE. The means are approximately two times larger than what was found in a previous study (Chambers and others, 2022, doi:10.1017/jog.2021.124) that assumed a sustained late-21st-century climate beyond 2100, demonstrating the importance of post-2100 climate trends on Antarctic mass changes in the 22nd and 23rd centuries.

1. Introduction

The ice sheets of Antarctica and Greenland are the largest potential contributors to future sea-level rise caused by global warming because of their enormous volumes. These amount to 57.9 ± 0.9 m SLE (sea-level equivalent) for the Antarctic ice sheet (AIS) (Morlighem and others, 2020) and 7.42 ± 0.05 m SLE for the Greenland ice sheet (GrIS) (Morlighem and others, 2017). Observations revealed that both ice sheets have been losing substantial amounts of mass since the 1990s. For the period 2012–2017, The IMBIE Team (2018) reported a mass loss of 219 ± 43 Gt a^{-1} for the AIS, most of which originates from the West Antarctic ice sheet (WAIS), and The IMBIE Team (2020) reported a loss of 244 ± 28 Gt a^{-1} for the GrIS (IMBIE: Ice sheet Mass Balance Inter-comparison Exercise). Therefore, the recent absolute losses are of similar size (likely somewhat larger for the GrIS), whereas the relative loss (compared to the total mass) is approximately 10 times smaller for the AIS compared to the GrIS. For both ice sheets, changes in the surface mass balance (SMB) as well as dynamic changes contribute to the mass loss.

A particular threat for the WAIS is that it may undergo a rapid, catastrophic disintegration through a process known as marine-ice-sheet instability (MISI) (e.g., Weertman, 1974; Mercer, 1978; Thomas and Bentley, 1978; Schoof, 2007). In contrast to the East Antarctic ice sheet (EAIS), large parts of the WAIS are grounded on a bed which is below sea level and sloping downward inland. Therefore, an initial retreat of the grounding line causes the ice sheet to be thicker at its new location, which may increase discharge and thus mass loss, so that the grounding line retreats even further in a runaway fashion. There is paleoclimatic evidence that the WAIS collapsed during past warm periods (Pollard and DeConto, 2009; Alley and others, 2015; Dutton and others, 2015; Gasson and others, 2016; Turney and others, 2020). Recent observations suggest that a new instability may already be in its initial phase (e.g., Joughin and others, 2014; Rignot and others, 2014; The IMBIE Team, 2018).

To estimate the future contribution of the AIS and GrIS to sea-level rise until the end of the 21st century, the Ice Sheet Model Intercomparison Project for CMIP6 (ISMIP6) was devised (Nowicki and others, 2016, 2020). It is part of the Coupled Model Intercomparison Project Phase 6 (CMIP6), a major international climate modelling initiative (Eyring and others, 2016) with the main goal to provide input for the recently published Sixth Assessment Report (AR6) of the Intergovernmental Panel on Climate Change (IPCC) (IPCC, 2021). For the AIS, when forced by output from CMIP5 global climate models (GCMs), a mass loss in the range of -7.8 to 30.0 cm SLE was found under the unabated warming pathway RCP8.5 [RCP: Representative Concentration Pathway] (Seroussi and others, 2020). The limited number of results for the reduced emissions pathway RCP2.6 fall within this range, and so do the results obtained with CMIP6 climate forcings (Payne and others, 2021). This rather unclear picture for the AIS is a consequence of the counteracting effects of mass loss due

© The Author(s), 2023. Published by Cambridge University Press on behalf of International Glaciological Society. This is an Open Access article, distributed under the terms of the Creative Commons Attribution licence (<http://creativecommons.org/licenses/by/4.0/>), which permits unrestricted re-use, distribution and reproduction, provided the original article is properly cited.

[cambridge.org/jog](https://www.cambridge.org/jog)



to ocean warming and mass gain from increased snowfall. The main findings for the GrIS, when forced by output from CMIP5 GCMs, were contributions of 90 ± 50 and 32 ± 17 mm SLE for RCP8.5 and RCP2.6, respectively (Goelzer and others, 2020). The CMIP6 GCMs tend to feature a warmer atmosphere, which results in higher mass loss due to increased surface melt (Payne and others, 2021).

The full suite of ISMIP6 experiments with both CMIP5 and CMIP6 forcings was carried out with the ice-sheet model SICOPOLIS ('Simulation COde for POLythermal Ice Sheets', www.sicopolis.net), as documented in detail by Greve and others (2020a, 2020b). Chambers and others (2022) extended the ISMIP6 simulations for the AIS with SICOPOLIS until the year 3000, assuming a sustained late-21st-century climate beyond 2100 (atmospheric forcing randomly sampled from the 10-year interval 2091–2100, oceanic forcing kept fixed at 2100 values). Compared to the uncertain response projected by the ISMIP6 ensemble over the 2015–2100 period, a radically different picture emerges, demonstrating that the long-term consequences of the high-emissions scenario RCP8.5/SSP5-8.5 [SSP: Shared Socioeconomic Pathway] are much greater than the 100-year response even if no further climate trend is applied beyond 2100. A similar study for the GrIS was conducted by Greve and Chambers (2022).

Other studies on the response of the AIS to longer-term climate change have also been conducted. Schaeffer and others (2012) and Levermann and others (2013) used statistical relationships between past temperatures and global sea levels to predict future sea-level change from all sources, including the ice sheets. Gollidge and others (2015) used the Parallel Ice-Sheet Model (PISM) to demonstrate that atmospheric warming in excess of 1.5 to 2°C above present, triggers ice-shelf collapse and a centennial to millennial-scale response by the AIS. They simulated a contribution to sea-level rise from Antarctica under higher emission scenarios of 0.6 to 3 m by the year 2300. Similarly, Garbe and others (2020) found that at greater than 2°C of global average warming, the WAIS is committed to long-term partial collapse. They also found distinct regimes in the rates of sea-level rise per degree, with a doubling in the rate if warming becomes greater than 2°C. Bulthuis and others (2019) carried out AIS projections until 3000 based on spatially uniform temperature-anomaly time-series and a combination of simulations with the fast Elementary Thermomechanical Ice Sheet (f.ETISH) model, an emulator, probabilistic methods and uncertainty quantification. They found that, irrespective of parametric uncertainty, the WAIS remains stable under RCP2.6, while RCP8.5 triggers its collapse under almost all investigated cases. In the ISMIP6-endorsed Antarctic BUttrressing Model Intercomparison Project (ABUMIP; Sun and others, 2020), the response of the AIS to sudden and sustained loss of ice shelves was simulated by an ensemble of 15 ice-sheet models. It was found that this leads to a multi-metre (1–12 m) contribution to sea-level rise over the 500-year-long simulations. Lowry and others (2021) used statistical emulation based on simulations with PISM to investigate the evolution of the AIS until 2300 under RCP8.5 and RCP2.6, assuming no further climate change beyond 2100 (similar to Chambers and others, 2022). The contribution to sea-level rise was found to be indistinguishable between the two pathways in the 21st century, while multi-metre differences occur in subsequent centuries. DeConto and others (2021) used their observationally calibrated ice-sheet-shelf model for simulations until 2100 and extended until 2300, employing extended RCP scenarios (Meinshausen and others, 2011). Their results demonstrate the possibility that rapid and unstoppable sea-level rise from the AIS will be triggered if Paris Agreement targets (limiting global mean warming in the 21st century to less than 2°C above pre-industrial levels) are exceeded. Lipscomb and others (2021)

used the Community Ice Sheet Model (CISM) to investigate the response of the AIS to ISMIP6 ocean thermal forcings only, extended to 2500. They found long-term retreat of the WAIS and showed that the Amundsen sector exhibits threshold behaviour with modest retreat or complete collapse, depending on parameter settings in the melt scheme, ocean forcing, and basal friction law. Complete collapse of the WAIS occurred under some combinations of low basal friction and high thermal forcing anomalies. Van Breedam and others (2020) projected the response of the AIS and GrIS 10 000 years into the future with the Earth system model of intermediate complexity LOVECLIMv1.3 (LOVECLIM: LOch-Vecode-Ecbilt-CLio-agIsm Model), including the ice-sheet model AGISM (Antarctic and Greenland Ice Sheet Model), forced by the extended concentration pathways ECP2.6, 4.5, 6.0 and 8.5 until 2300 and zero emissions thereafter. For the AIS, they report mass losses ranging from about 1.6 m SLE for the lowest forcing scenario until up to 27 m SLE for the higher-forcing scenarios.

In the present study, we follow an approach similar to Chambers and others (2022), extending the ISMIP6-Antarctica simulations further into the future. However, we drop the assumption of a sustained climate with no warming or cooling trend beyond 2100. Instead, to account for greenhouse-gas emissions pathways and climate inertia after the 21st century, we construct extensions of all ISMIP6-Antarctica climate forcings until 2300 by a climate-index method explained in Sect. 2. The set-up of SICOPOLIS and the 18 model experiments (1 control, 14 RCP8.5/SSP5-8.5, 3 RCP2.6/SSP1-2.6) are explained in Sect. 3. The results are described in Sect. 4, and a discussion and conclusion is provided in Sect. 5.

2. Climate forcing

We construct an ensemble of climate forcings for Antarctica for the period 2015–2300 by combining results from MIROC4m (MIROC: Model for Interdisciplinary Research On Climate) RCP8.5 and RCP4.5 simulations for 1995–2300 (partially published in Bakker and others, 2016) with the ensemble of ISMIP6 forcings for 2015–2100 (Nowicki and others, 2020; Seroussi and others, 2020; Payne and others, 2021). To do so, we derive a set of atmospheric and oceanic climate indices from the MIROC4m simulations such that 1995–2014 averages of the considered fields are mapped to zero and 2091–2100 averages to unity (Sect. 2.1). We then use the climate indices to extrapolate the ensemble of ISMIP6 forcings to the period 2101–2300 (Sect. 2.2). Together with the original ISMIP6 forcings, this method provides smooth climate forcings for the entire period 2015–2300. Beyond the needs of this study, the method is applicable in general to extend climate forcings of limited duration further into the future.

2.1. Climate indices

We define five atmospheric and one oceanic climate indices. For the atmosphere, the considered fields are the mean-annual surface temperature (ST), summer (December–January–February, DJF) surface temperature (ST_DJF), precipitation (prec), evaporation (evap) and surface runoff (roff). ST and SMB = prec – evap – roff define the atmospheric forcing, while ST_DJF is required for the parameterization of ice-shelf collapse (see the last part of Sect. 2.2).

All fields are spatially averaged over the AIS land grid (excluding the ice shelves because they are not contained in the MIROC4m set-up), and then mapped linearly on a dimensionless scale such that

$$\begin{aligned} c_{xx}(1995\text{--}2014 \text{ average}) &= 0, \\ c_{xx}(2091\text{--}2100 \text{ average}) &= 1, \end{aligned} \quad (1)$$

where $xx \in \{ST, ST_DJF, prec, evap, roff\}$. This yields the five atmospheric climate indices c_{ST} , c_{ST_DJF} , c_{prec} , c_{evap} and c_{roff} .

For the ocean, we use the average temperature south of 62.5°S and between 200 and 800 metres depth. This domain encompasses the Southern Ocean surrounding the ice-shelf cavities and a range of typical ice-shelf drafts where basal melting takes place. Non-dimensionalization with the same pinning points as defined by Eqn. (1) ($xx = oc$) provides the oceanic climate index c_{oc} .

Since the MIROC4m results are available for RCP8.5 and RCP4.5, the above method provides climate indices for these two pathways. However, ISMIP6 covers RCP8.5 and RCP2.6, so that we also require the climate indices for RCP2.6. To obtain these, we extrapolate the atmospheric and oceanic indices for RCP8.5 and RCP4.5, assuming linear relations between the indices and the radiative forcing of the RCP scenarios:

$$c_{xx}^{RCP2.6} = c_{xx}^{RCP4.5} - \frac{4.5 - 2.6}{8.5 - 4.5} \times (c_{xx}^{RCP8.5} - c_{xx}^{RCP4.5}). \quad (2)$$

The resulting climate indices are shown in Fig. 1. For RCP8.5, the change of all six variables during the 22nd and 23rd century goes well beyond late-21st-century levels. The five atmospheric indices evolve into a certain saturation towards the end of the period, whereas the oceanic index increases steadily. This is due to the larger inertia of the ocean compared to the atmosphere. For RCP2.6, the atmospheric indices largely fall below their late-21st-century levels, indicating a partial recovery of the climate change. By contrast, the oceanic index does not

show such a recovery and keeps on increasing (albeit at a decreasing rate), which again results from the larger oceanic inertia.

2.2. Scaling of the ISMIP forcings

The ISMIP6 forcings for the AIS consist of anomalies for the surface temperature [$\Delta ST(x, y, t)$] and the SMB [$\Delta SMB(x, y, t)$] relative to 1995–2014, and absolute values for the oceanic thermal forcing [$TF(x, y, z, t)$], all for the period 2015–2100. These were derived from a systematic sampling of CMIP5 GCMs that reflects their spread in future projections (Barthel and others, 2020), while CMIP6 GCMs were added mostly on the basis of availability (Payne and others, 2021). The atmospheric forcings ΔST and ΔSMB enter the ice-sheet simulations directly as upper boundary conditions. By contrast, TF is used to compute sub-ice-shelf melt rates via a non-local quadratic parameterization ('ISMIP6 standard approach') calibrated by observations (Jourdain and others, 2020).

To extend the ISMIP6 forcings until 2300, the oceanic thermal forcing is converted to an anomaly as well by subtracting the 1995–2014 mean:

$$\Delta TF(x, y, z, t) = TF(x, y, z, t) - TF_{1995-2014}(x, y, z), \quad (3)$$

$$t \leq 2100 \text{ CE.}$$

We then scale the anomalies by using the MIROC4m-derived climate indices as follows:

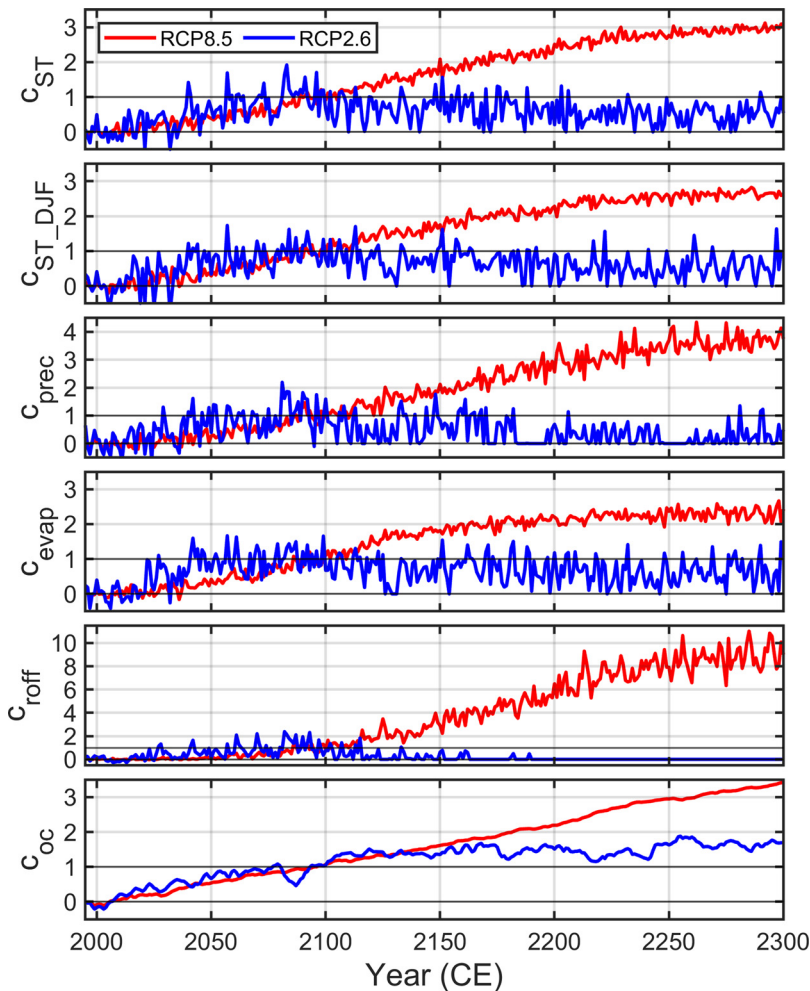


Figure 1. RCP8.5 and RCP2.6 climate indices for the mean-annual surface temperature (c_{ST}), DJF surface temperature (c_{ST_DJF}), precipitation (c_{prec}), evaporation (c_{evap}), surface runoff (c_{roff}) and ocean temperature (c_{oc}), derived from MIROC4m simulations until the year 2300. Note that the scaling defined by Eqn. (1) implies that any non-zero value or variability of the indices corresponds to a stronger climate change for RCP8.5 than for RCP2.6.

$$\begin{aligned}
 \Delta ST(x, y, t) &= c_{ST}(t) \times \Delta ST_{2091-2100}(x, y), \\
 \Delta prec(x, y, t) &= c_{prec}(t) \times \Delta prec_{2091-2100}(x, y), \\
 \Delta evap(x, y, t) &= c_{evap}(t) \times \Delta evap_{2091-2100}(x, y), \\
 \Delta roff(x, y, t) &= c_{roff}(t) \times \Delta roff_{2091-2100}(x, y), \\
 \Delta TF(x, y, z, t) &= c_{oc}(t) \times \Delta TF_{2091-2100}(x, y, z),
 \end{aligned} \tag{4}$$

$t > 2100$ CE,

where $\Delta prec$, $\Delta evap$ and $\Delta roff$ are the anomalies of precipitation, evaporation and runoff, respectively, and the subscripts ‘2091–2100’ denote the mean values over this decade. The anomaly ΔSMB results from

$$\begin{aligned}
 \Delta SMB(x, y, t) &= \Delta prec(x, y, t) - \Delta evap(x, y, t) \\
 &\quad - \Delta roff(x, y, t),
 \end{aligned} \tag{5}$$

$t > 2100$ CE,

and ΔTF is converted back to absolute values:

$$TF(x, y, z, t) = TF_{1995-2014}(x, y, z) + \Delta TF(x, y, z, t), \tag{6}$$

$t > 2100$ CE.

Thus, this method provides extended ISMIP6 forcings for the AIS [$\Delta ST(x, y, t)$, $\Delta SMB(x, y, t)$, $TF(x, y, z, t)$] until the year 2300. Table 1 shows the magnitude of the atmospheric and oceanic forcing for all GCMs considered here. A noteworthy aspect is that the cumulative SMB anomaly can be both positive and negative. This is a consequence of the counteracting effects of increasing loss (runoff, evaporation), but also increasing precipitation due to larger moisture transport by the warmer air. The different GCMs predict a different net effect on the SMB, ranging from distinctly positive to distinctly negative.

While the climate indices are based on results from a single GCM (MIROC4m), a strength of our method is that it does not depend much on the sensitivity of this particular model to changed external forcing (‘climate sensitivity’). This is so because of the normalization carried out by Eqn. (1), which eliminates at least the linear part of the climate sensitivity: computing the indices with a different GCM that is, for instance, twice as sensitive as MIROC4m (produces a climate signal twice as strong) would produce exactly the same result. Differences can only arise from

Table 1. Mean surface temperature anomaly ($\overline{\Delta ST}$), cumulative SMB anomaly ($c\Delta SMB$) and mean oceanic thermal forcing (\overline{TF}) for the period 2015–2300 and all climate forcings of this study

GCM	Scenario	$\overline{\Delta ST}$ (°C)	$c\Delta SMB$ (m ice equiv.)	\overline{TF} (°C)
< For the core experiments (Tier 1) >				
NorESM1-M	RCP8.5	5.667	15.510	2.209
MIROC-ESM-CHEM	RCP8.5	10.157	−6.325	1.442
NorESM1-M	RCP2.6	0.194	0.286	0.539
CCSM4	RCP8.5	9.511	19.375	1.652
< For the extended ensemble (Tier 2) >				
HadGEM2-ES	RCP8.5	9.141	−62.238	2.391
CSIRO-Mk3.6.0	RCP8.5	9.654	33.240	1.381
IPSL-CM5A-MR	RCP8.5	6.351	23.166	1.247
IPSL-CM5A-MR	RCP2.6	0.515	0.612	0.709
< For the CMIP6 extension (Tier 2) >				
CNRM-CM6-1	SSP5-8.5	12.435	44.911	1.927
CNRM-CM6-1	SSP1-2.6	1.245	2.587	0.827
UKESM1-0-LL	SSP5-8.5	11.102	−20.363	2.196
CESM2	SSP5-8.5	12.849	−22.145	1.613
CNRM-ESM2-1	SSP5-8.5	10.162	35.427	2.091

$\overline{\Delta ST}$ and $c\Delta SMB$ spatially averaged over the present-day AIS (including ice shelves), \overline{TF} spatially averaged over the ice-shelf areas and the depth interval 200–800 m. Anomalies relative to 1995–2014 means of the reference climatology.

nonlinear effects (different responses of other GCMs to longer-term radiative forcing *relative to 2100 anomalies*) and different internal variabilities. The extrapolation of Eqn. (2) makes sure that the normalization also holds for RCP2.6, even though we do not have MIROC4m results for this pathway. Therefore, the extrapolation, even though ad hoc, is not too critical. It mainly affects the long-term behaviour, for which it produces the plausible result that, while for RCP8.5 climate change continues beyond 2100, for RCP2.6 a partial recovery occurs.

In the supplementary document, we apply for RCP8.5 the MIROC4m-derived climate indices on the MIROC4m climate fields (surface temperature, ocean temperature at 450 m depth, precipitation) themselves, which allows a direct comparison of originally computed and extrapolated results. This exercise shows that, overall, the climate-index method performs reasonably well, but also identifies a source of uncertainty from regional, nonlinear effects that cannot be captured by the method.

For one of the ISMIP6 simulations (CCSM4/RCP8.5), an additional ice-shelf-collapse forcing is employed. It stipulates that ice-shelf collapse occurs when the mean surface melting over the past decade exceeds a threshold value of 725 mm water equiv. a^{−1} (Trusel and others, 2015; Seroussi and others, 2020). Hereby, the mean surface melting is parameterized by an exponential function of the DJF (austral summer) near-surface air temperature, ST_DJF . For $t \leq 2100$ CE, ST_DJF is taken from bias-adjusted, GCM-forced simulations with the regional climate model RACMO2 (Trusel and others, 2015). For $t > 2100$ CE, we construct ST_DJF via its anomaly, ΔST_DJF , as follows:

$$\begin{aligned}
 \Delta ST_DJF(x, y, t) &= c_{ST_DJF}(t) \times \Delta ST_{2091-2100}(x, y), \\
 ST_DJF(x, y, t) &= ST_{1995-2014}(x, y) \\
 &\quad + [ST_DJF_{param}(x, y) - ST_{param}(x, y)] \\
 &\quad + \Delta ST_DJF(x, y, t),
 \end{aligned}$$

$t > 2100$ CE. (7)

Note that $\Delta ST_{2091-2100}$ and $ST_{1995-2014}$ are mean-annual rather than DJF values because only these are available in the ISMIP6 forcing. To convert to DJF, we use the parameterized difference [$ST_DJF_{param} - ST_{param}$] of present-day DJF and mean-annual temperatures, respectively, by Fortuin and Oerlemans (1990) (see also Greve and others, 2020a, their Eqs. (10) and (11)).

This method provides annual ice-shelf-collapse masks for the years 2101–2300. To guarantee a smooth transition to the pre-2100 masks provided by ISMIP6, we define a 10-year interval 2101–2110, during which the final masks are computed as weighted averages between the original ISMIP6 masks and our extended ones.

3. Model experiments

We apply the ice-sheet model SICOPOLIS (SICOPOLIS Authors, 2021) to the AIS with hybrid shallow-ice–shelvy-stream dynamics (Bernales and others, 2017) for grounded ice, shallow-shelf dynamics for floating ice, a Weertman-Budd-type sliding law tuned separately for 18 different regions (Greve and others, 2020a), and ice thermodynamics treated by the one-layer melting-CTS enthalpy scheme (CTS: cold-temperate transition surface; Blatter and Greve, 2015; Greve and Blatter, 2016). The horizontal resolution is 8 km, which, in combination with the sliding law that features a continuous basal drag across the grounding line, is sufficient to produced good results for the grounding line migration in both advance and retreat scenarios (Gladstone and others, 2017; Chambers and others, 2022). In the vertical, we use terrain-following coordinates (σ)

Table 2. Extended ISMIP6-Antarctica Tier-1 and 2 future climate experiments for the period 2015–2300 discussed in this study

#	GCM	Scenario	Ocean forcing	Ice-shelf fracture
< Control experiment >				
0	-	ctrl_proj	-	-
< Core experiments (Tier 1) >				
5	NorESM1-M	RCP8.5	Medium	No
6	MIROC-ESM-CHEM	RCP8.5	Medium	No
7	NorESM1-M	RCP2.6	Medium	No
8	CCSM4	RCP8.5	Medium	No
9	NorESM1-M	RCP8.5	High	No
10	NorESM1-M	RCP8.5	Low	No
12	CCSM4	RCP8.5	Medium	Yes
13	NorESM1-M	RCP8.5	PIGL-Medium	No
< Extended ensemble (Tier 2) >				
A5	HadGEM2-ES	RCP8.5	Medium	No
A6	CSIRO-Mk3.6.0	RCP8.5	Medium	No
A7	IPSL-CM5A-MR	RCP8.5	Medium	No
A8	IPSL-CM5A-MR	RCP2.6	Medium	No
< CMIP6 extension (Tier 2) >				
B6	CNRM-CM6-1	SSP5-8.5	Medium	No
B7	CNRM-CM6-1	SSP1-2.6	Medium	No
B8	UKESM1-0-LL	SSP5-8.5	Medium	No
B9	CESM2	SSP5-8.5	Medium	No
B10	CNRM-ESM2-1	SSP5-8.5	Medium	No

See Nowicki and others (2020) for references for the GCMs.

transformation) with 81 layers in the ice domain and 41 layers in the thermal lithosphere layer below. For details on the set-up, the initialization procedure by a paleoclimatic spin-up, comparisons between the simulated and observed ice thickness and surface velocity for our initialization year 1990, as well as the historical run ('hist') that bridges the gap between 1990 and the start date of the projections in January 2015 by employing NorESM1-M/RCP8.5 SMB, surface temperature (ST) and oceanic thermal forcing (TF), we refer to Greve and others (2020a). From the last 20 years of the historical run, we extract the 1995–2014 climatology (SMB, ST) required as a reference for the future climate experiments.

An overview of our extended ISMIP6 experiments is given in Table 2. The method of extending the ISMIP6 climate forcing until 2300 is described above (Sect. 2). 14 experiments are for the 21st-century unabated warming pathway RCP8.5 (CMIP5) / SSP5-8.5 (CMIP6), and three are for the reduced emissions pathway RCP2.6 (CMIP5) / SSP1-2.6 (CMIP6) that is largely in line with the commitments of the Paris Agreement (maintaining the global mean temperature well below a 2°C increase above pre-industrial levels). In two of the RCP8.5 experiments, the impact of different calibrations of the parameterization for sub-ice-shelf melting ('high' and 'low' vs. the normal, 'medium' calibration, thereby exploring the uncertainty of the parameterization) is tested, and one experiment employs a calibration in which only observed basal-melt values near the grounding line of the Pine Island ice shelf are used ('PIGL-medium') (Jourdain and others, 2020). As already mentioned in Sect. 2.2, in one experiment, ice-shelf fracture triggered by surface melting is accounted for. In addition, a projection control simulation ('ctrl_proj') employs constant climate conditions based on the 1995–2014 reference climatology.

4. Results

The simulated mass change of the AIS, expressed as a sea-level contribution, is shown in Fig. 2. For the control run ctrl_proj, the ice sheet remains stable, showing only a minimal mass loss of 3.49 mm SLE during the 286 years model time. This stability also holds for the longer control run over a 986-years period until the year 3000 reported by Chambers and others (2022).

Until 2100, the future projections are equivalent to the original ISMIP6-Antarctica simulations carried out with SICOPOLIS (Seroussi and others, 2020; Greve and others, 2020a; Payne and others, 2021), characterized by a range of uncertainties from a notable mass loss to a slight mass gain and no clear separation between RCP8.5/SSP5-8.5 (mean ± 1-sigma range: 32.6 ± 67.2 mm SLE) and RCP2.6/SSP1-2.6 (8.4 ± 15.9 mm SLE). [Note: The values for RCP8.5/SSP5-8.5 differ from those given

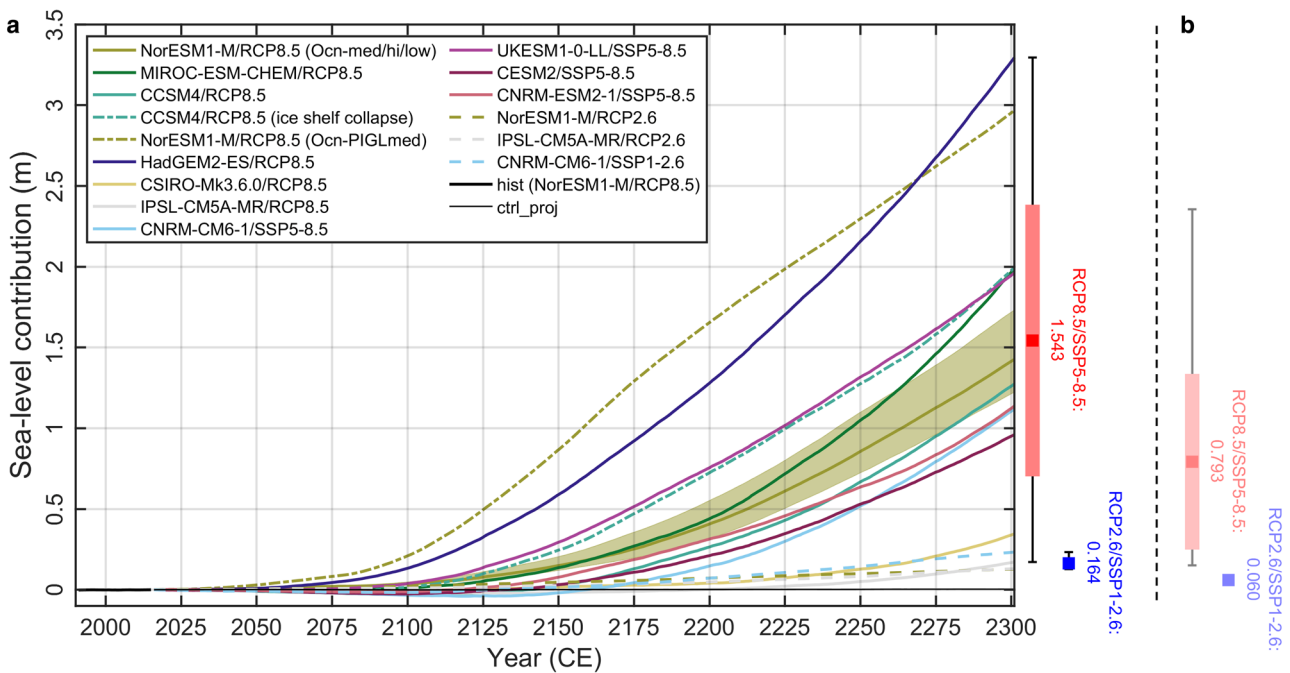


Figure 2. (a) ISMIP6-Antarctica historical run (hist), projection control run (ctrl_proj) and Tier-1 and 2 future climate experiments extended until 2300: Simulated ice mass change, counted positively for loss and expressed as a sea-level contribution. Experiments in the legend grouped such that RCP8.5/SSP5-8.5 comes first and RCP2.6/SSP1-2.6 thereafter, otherwise like in Table 2. The red and blue boxes to the right show the 2300 means for RCP8.5/SSP5-8.5 and RCP2.6/SSP1-2.6, respectively (RCP8.5/SSP5-8.5: also ± 1-sigma); the whiskers show the corresponding full ranges. (b) Same 2300 statistics, but for the results by Chambers and others (2022) without a further warming trend beyond 2100.

by Greve and others (2020a) because that study excluded Exp. 13 (NorESM1-M/RCP8.5 with ‘PIGL-medium’ calibration) for the computation, which we have included here.] However, a different picture emerges in the longer term. By 2300, the ice sheet ends up losing mass for all cases, and it responds much more strongly to the ensemble of RCP8.5/SSP5-8.5 simulations than to the RCP2.6/SSP1-2.6 simulations. The final mass loss amounts to 1.54 ± 0.84 m SLE for RCP8.5/SSP5-8.5, while it is limited to 0.164 ± 0.049 m SLE for RCP2.6/SSP1-2.6. The mean values for both pathways are approximately twice as large as those found by Chambers and others (2022) for a sustained late-21st-century climate (no further warming trend) beyond 2100 (Fig. 2b).

The influence of the ice mass loss due to oceanic forcing is explored by Exps. 5, 9, 10 (NorESM1-M/RCP8.5 with ‘medium’, ‘high’ and ‘low’ calibration, respectively). The results are shown by the olive lines and olive-shaded regions in Fig. 2. By 2300, the simulated mass loss is $1.43^{+0.31}_{-0.20}$ m SLE. Thus, the uncertainty due to these three calibrations is significant, but smaller than the uncertainty due to the GCM forcings. A more extreme test is Exp. 13, which is NorESM1-M/RCP8.5 with the ‘PIGL-medium’ calibration. Until the mid-22nd century, this leads to an, on average, ~ 2 times larger total ice-shelf basal melting than for Exp. 5 (later on, the difference becomes smaller due to ice-shelf decay). It has a pronounced effect on the mass loss of the ice sheet: By 2300, it is 2.97 m SLE compared to the initial 1990 state, more than doubling that of Exp.5. This highlights the great sensitivity of the AIS to oceanic forcing.

Exps. 8 and 12 (CCSM4/RCP8.5) investigate the influence of ice-shelf hydrofracture as described above (included in Exp. 12). Exp. 8 is actually one of the cases that produce a mass gain of the ice sheet during the 21st century. Adding ice-shelf hydrofracture via the time-dependent collapse mask in Exp. 12 reverts this behaviour to a mass loss. By 2300, both experiments produce a loss, which is 1.27 m SLE for Exp. 8, but 2.00 m SLE for Exp. 12. Thus, the process can act as a significant amplifier of the mass loss of the AIS.

In Fig. 3, the sea-level contributions by 2300 are shown separately for the regions of the EAIS, the WAIS and the Antarctic Peninsula (AP). Averaged across all the high-emission cases (panel a), the WAIS contributes 1.28 m SLE, compared with just 0.24 m SLE from the EAIS and 0.019 m SLE from the AP. This contrasts with the low-emission cases (panel b) which have average SLE contributions from the WAIS and EAIS of 0.064 and 0.097 m, respectively, with the AP contribution being very slightly negative at -0.00078 m. These findings agree with

those by Chambers and others (2022) (simulations until 3000, no further warming or cooling trend beyond 2100), and the reason for the predominant contribution from the WAIS for RCP8.5/SSP5-8.5 is that it undergoes a collapse in the areas of the Amundsen Sea Embayment and the Siple Coast where the bedrock bathymetry deepens inward. We cannot decide whether this modelled collapse is a ‘classical’ MISI (unstable and irreversible retreat driven by an internal instability mechanism), or whether it is a more direct response to the loss of ice-shelf buttressing (Haseloff and Sergienko, 2018; Gudmundsson and others, 2019). However, either way, the result is a rapid mass loss from the WAIS. By contrast, the weaker climatic forcings of RCP2.6/SSP1-2.6 do not trigger a WAIS collapse in our simulations.

Figure 4 shows the components of the global mass balance (integrated over the ice sheet, all counted as positive for mass gain): SMB, basal mass balance (BMB), calving and ice volume change (dV/dt). For the RCP8.5/SSP5-8.5 means (thick lines in the figure), the ice sheet keeps losing volume (\propto mass) over the entire period and at an accelerating rate of change. The SMB, driven by the counteracting effects of increasing precipitation and increasing runoff, remains positive throughout the model time, even with a slight increase. The BMB, predominantly produced by sub-ice-shelf melting, strongly increases in magnitude over time, which is the main reason for the accelerated volume loss of the ice sheet. The essentially monotonic increase (except for short-term fluctuations) of the BMB contrasts with the study by Chambers and others (2022) where it peaks around 2100, but then falls back to values around $-4 \times 10^{12} \text{ m}^3 \text{ a}^{-1}$ between 2150 and 2300. Calving into the surrounding ocean (that results from a 50-m ice-thickness threshold; Greve and others, 2020a) is also a significant component of the mass balance. However, it changes only moderately over time. The inter-annual variability of the volume change is mainly due to that of the SMB and, to a lesser extent, the BMB, which reflects the variability of the atmospheric and oceanic forcings.

The mass balance components feature significant variabilities across the individual experiments. In some cases, the SMB falls below its initial level, episodically even becoming negative. This can happen if the stabilizing effect of increasing precipitation is less pronounced in the respective climate forcing. The greatest outlier for BMB, with strongly elevated negative values during the late 21st and the 22nd century, is Exp. 13 (NorESM1-M/RCP8.5). This is a consequence of the ‘PIGL’ calibration of ice-shelf basal melting based on observations close to the grounding line of Pine Island Glacier, which is used for this experiment only,

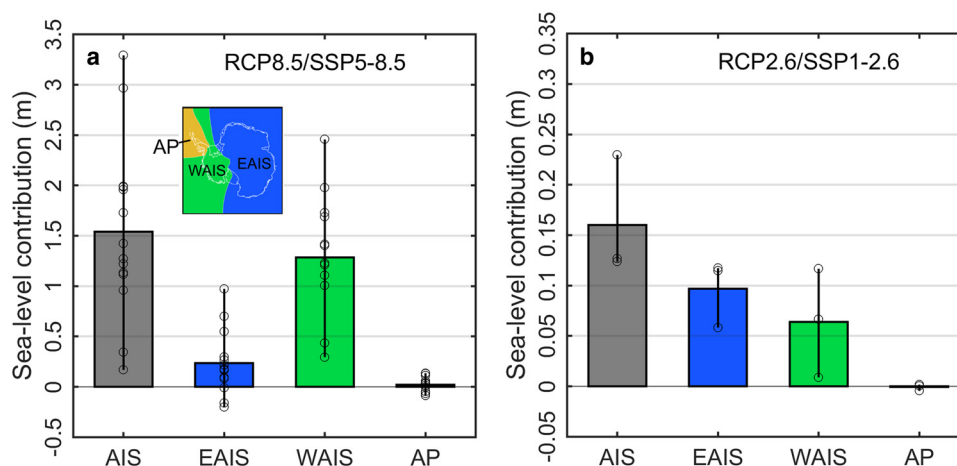


Figure 3. Simulated sea-level contribution for the entire ice sheet and three regions (EAIS, WAIS, AP; shown in the inset) by the year 2300 relative to *ctrl_proj*, for (a) the RCP8.5/SSP5-8.5 and (b) the RCP2.6/SSP1-2.6 ensemble. The whiskers show the full range of sea-level contributions across the simulations that make up the means, and the circles on the whiskers show the result for each simulation. Note that the y-axis ranges are different by a factor of 10.

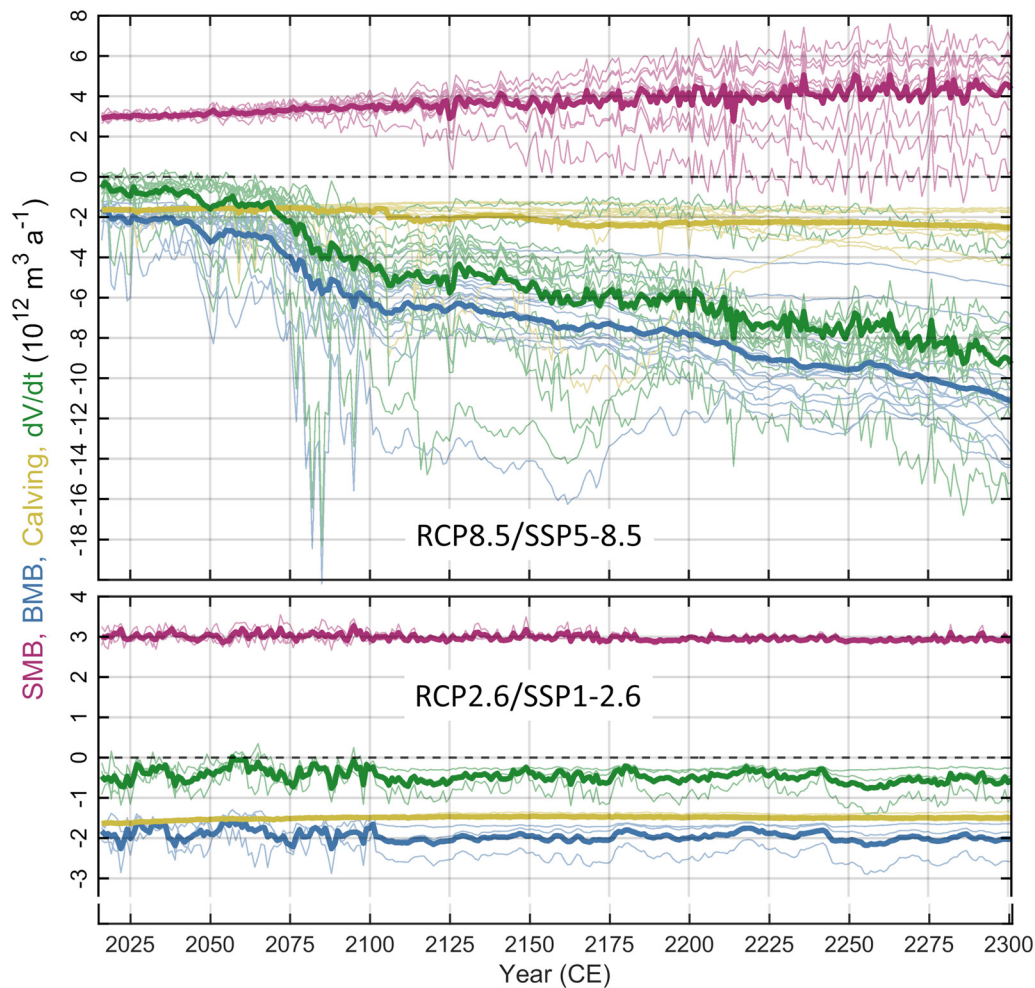


Figure 4. Main components of the global mass balance for the RCP8.5/SSP5-8.5 and RCP2.6/SSP1-2.6 experiments: Surface mass balance (SMB, purple), basal mass balance (BMB, blue), calving (yellow) and ice volume change (dV/dt , green). Thick lines are the respective means, thin lines the individual results for the fourteen RCP8.5/SSP5-8.5 and three RCP2.6/SSP1-2.6 experiments.

whereas for all other experiments, the calibration is based on circum-Antarctic observations (Jourdain and others, 2020; Seroussi and others, 2020). A similar outlier for calving is Exp. 12 (CCSM4/RCP8.5), the only experiment for which an explicit parameterization for ice-shelf fracture (assumed to be caused by large amounts of liquid water ponding at the surface of ice shelves) is employed (Trusel and others, 2015; Seroussi and others, 2020).

Regarding the RCP2.6/SSP1-2.6 means, no significant trend in any of the mass balance components can be seen during the model period. Apart from short-term fluctuations, the initial imbalance (negative dV/dt) remains essentially constant. In contrast to RCP8.5/SSP5-8.5, where BMB clearly dominates, the losses due to BMB and calving are of similar size. Approximately 85% of the combined loss is compensated by the positive SMB, so that only a limited residual imbalance remains. The variability across the RCP2.6/SSP1-2.6 experiments is less pronounced than what we have seen for RCP8.5/SSP5-8.5. The significance of this statement is limited, though, because of the smaller number of experiments. However, one interesting observation is that the CMIP6-forced Exp. B7 (CNRM-CM6-1/SSP1-2.6) produces a notably larger BMB, and thus dV/dt , than the two CMIP5-forced Exps. 7 and A8.

We now discuss in more detail the results of Exp. 6 (MIROC-ESM-CHEM/RCP8.5), which was already focused on in the previous study by Chambers and others (2022). It features high atmospheric changes and median ocean warming compared

to the other CMIP5 GCMs (Barthel and others, 2020), and it produces a $\sim 29\%$ above average mass loss of 1.99 m SLE (WAIS 1.69 m, EAIS 0.16 m, AP 0.13 m) for our combined CMIP5/CMIP6 ensemble. The residual of the global mass balance, $Res = |SMB + BMB + Calving - dV/dt|$, has a mean value of $2.14 \times 10^4 \text{ m}^3 \text{ a}^{-1}$ over the 286 years simulation time. This is eight orders of magnitude smaller than the typical range of values of the individual components [$\mathcal{O}(10^{12} \text{ m}^3 \text{ a}^{-1})$, see Fig. 4], so that the model conserves mass very well (see also Calov and others, 2018).

Snapshots of the simulated ice thickness and surface velocity for Exp. 6 are shown in Fig. 5. By 2095, the ice sheet has overall undergone only minor changes compared to the initial year 2015, corresponding to a mass loss of 0.0070 m SLE. By 2195, which is just after the calving event mentioned above, the changes are more notable (mass loss 0.40 m SLE). A large part of the present-day Ross Ice Shelf has disappeared, and the grounding lines in the areas of the Pine Island and Thwaites glaciers and the Siple Coast have migrated inland, along with a speed-up of the ice streams. A similar, yet less pronounced grounding line retreat and speed-up has occurred in the area of Totten Glacier, and the northern part of the Amery Ice Shelf has disintegrated. By the end of 2300 (mass loss 1.99 m SLE), the collapse of the WAIS is progressing in full force, with dramatic retreats of the Pine Island/Thwaites and Siple Coast grounding lines, accompanied by additional retreats of the grounding line of the Filchner-Ronne Ice Shelf. In the EAIS, the Amery Ice Shelf has disappeared almost entirely, and the area of Totten Glacier shows some more

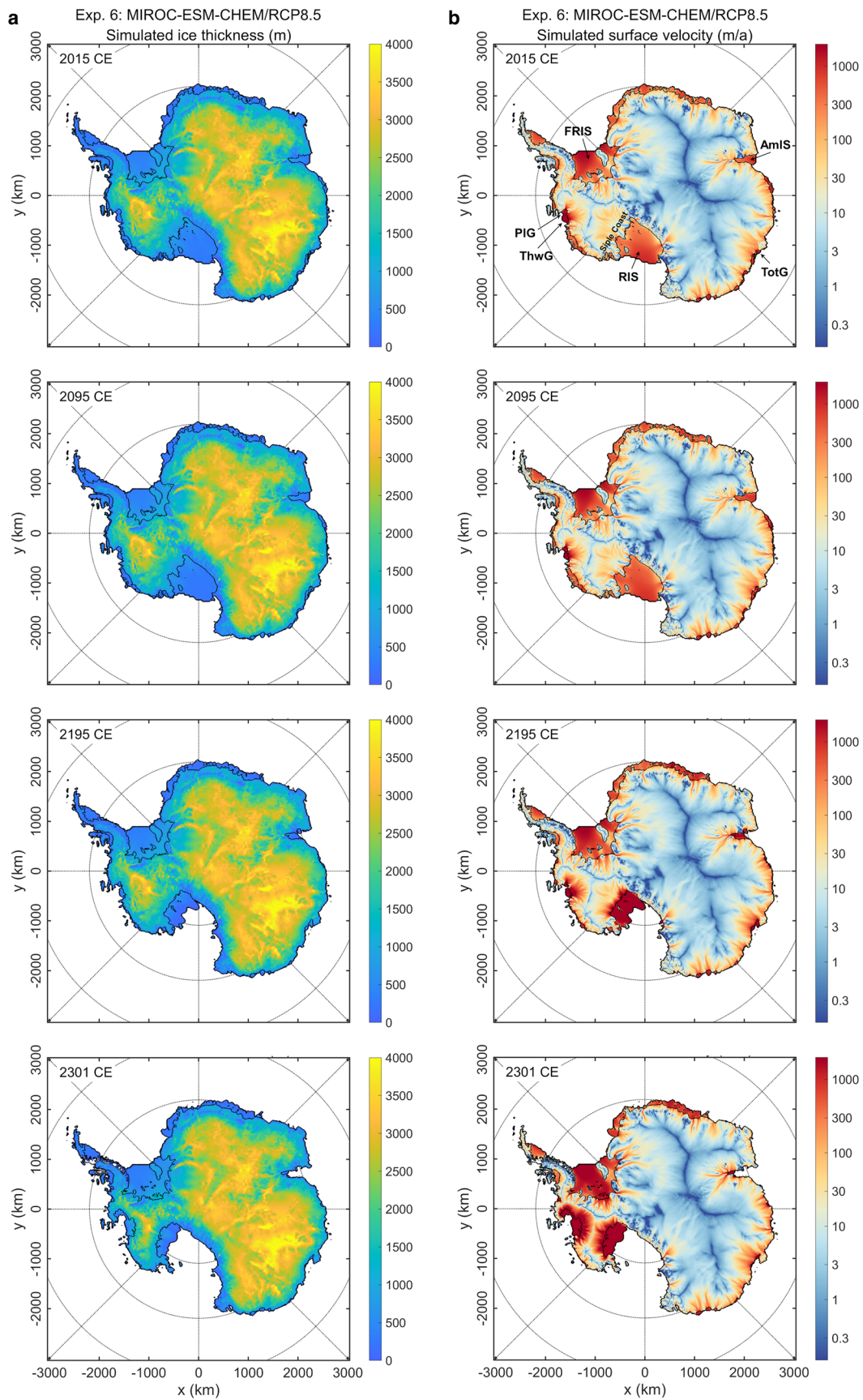


Figure 5. Snapshots of (a) the simulated ice thickness and (b) the surface velocity for Exp. 6 (MIROC-ESM-CHEM/RCP8.5) for the years 2015, 2095, 2195 and 2301 (i.e., the end of 2300). Spacing of the latitude circles is 10° , spacing of the longitude rays is 45° . RIS: Ross Ice Shelf, FRIS: Filchner–Ronne Ice Shelf, AmIS: Amery Ice Shelf, PIG: Pine Island Glacier, ThwG: Thwaites Glacier, TotG: Totten Glacier.

grounding line retreat; however, with limited impact on the ice sheet further inland.

5. Discussion and conclusion

The future climate simulations for the AIS until the year 2300 carried out in the present study reveal a different picture compared to the original ISMIP6-Antarctica simulations for the 21st century (Seroussi and others, 2020; Greve and others, 2020a; Payne and others, 2021). The latter produced a range of mass changes from a small gain (due to precipitation increases) to a moderate loss, and no clear distinction between the unabated warming (RCP8.5/SSP5-8.5) and reduced emissions pathways (RCP2.6/SSP1-2.6). By contrast, in our extended simulations, by 2300 mass gains of the AIS do not occur any more, and the mass loss under RCP8.5/SSP5-8.5 is substantially larger than that under RCP2.6/SSP1-2.6 (mean values of ~ 1.5 m SLE vs. only ~ 0.16 m SLE). In terms of the mean ± 1 -sigma mass loss range, RCP8.5/SSP5-8.5 becomes disjoint from RCP2.6/SSP1-2.6 around the year 2208. For comparison, Lowry and others (2021) report for their projections, based on a statistical emulator, 'likely' and 'very likely' times of emergence (significant separation between the RCP8.5 and RCP2.6 ensembles) of 2116 and 2189, respectively. Most of the mass loss under RCP8.5/SSP5-8.5 originates from the WAIS, which suffers a collapse in almost all simulations.

Compared to the previous study by Chambers and others (2022) in which a sustained late-21st-century climate beyond 2100 was assumed, the response of the AIS to our extrapolated climate-change scenarios is about two times larger by 2300 for both pathways. For RCP8.5/SSP5-8.5, this stronger response is immediately to be expected because, as detailed in Sect. 2.1, all climate indices are well above unity during the 22nd and 23rd century, which means that climate change becomes ever more serious. For RCP2.6/SSP1-2.6, the situation is different because the atmospheric climate recovers to below late-21st-century levels (all five indices), while only the oceanic climate index stays above unity after 2100. Evidently, the impact of the increasing oceanic forcing outweighs that of the recovering atmospheric forcing, so that mass loss due to sub-ice-shelf melt and subsequently enhanced drainage of grounded ice is the dominant process.

The threat of a WAIS instability under future climate change has already been expressed by a number of previous studies (see Sect. 1 for more details). A particular feature of the ISMIP6-Antarctica set-up for SICOPOLIS is that it applies an SMB correction to keep the ice sheet stable and close to observed conditions in the recent past (Greve and others, 2020a). This SMB correction has significant additional accumulation in the area of the Pine Island and Thwaites glaciers to prevent them from becoming unstable even before the end of the spin-up simulations. It is possible that this procedure over-stabilizes the area, so that the onset of the instability originating from there could be delayed. On the other hand, SICOPOLIS is quite sensitive to sub-ice-shelf melting compared to other ice-sheet models (Edwards and others, 2021). This factor facilitates the development of an instability because it makes the ice sheet more sensitive to grounding-line migration.

As already discussed by Chambers and others (2022), a weakness of the ISMIP6-type simulations is that the atmospheric forcing is not affected by the changing geometry of the ice sheet. While the ocean thermal forcing, TF, is three-dimensional and thus changes as the ice shelves become thicker or thinner, the atmospheric forcing fields, ΔST and ΔSMB , are 2D fields that were derived by GCMs under the assumption of a static, present-day ice sheet. Therefore, they do not change as the ice-surface elevation rises or falls. A possible improvement, also beneficial for

the resolution of the forcing fields, is to reprocess the GCM output by a regional climate model and compute vertical gradients of ST and SMB, so that at least a linearized feedback can be implemented (Franco and others, 2012). Such a method was employed for the ISMIP6-Greenland simulations and derived work (Goelzer and others, 2020; Nowicki and others, 2020; Greve and Chambers, 2022). Short of very demanding and computationally expensive fully coupled climate-ice-sheet simulations, a further possibility is to involve snapshots of climate-model results combined with more refined parameterizations for the climatic forcing, similar to the approach by Abe-Ouchi and others (2013) for the paleoglaciation of the Northern Hemisphere.

A weakness of the climate indices we used to extrapolate the ISMIP6 forcings until 2300 is that the method relies on the projections of a single GCM (MIROC4m) which will influence the forcings after 2100. However, as explained in Sect. 2.2, we do not consider this limitation too critical due to the normalization carried out by Eqn. (1), which eliminates the linear part of the climate sensitivity. Nevertheless, it would be worthwhile to investigate this issue quantitatively based on results from other GCMs for which extended projections until 2300 are available. For the ISMIP6 follow-up initiative 'ISMIP6 Projections 2300 Antarctica' (see below), climate forcings until 2300 are provided from four GCMs for RCP8.5/SSP5-8.5, and from one GCM for SSP1-2.6. These could be used for the purpose, including checking the validity of our extrapolation from RCP8.5 and RCP4.5 to RCP2.6 specified by Eqn. (2). We consider such a detailed investigation of the climate-index method to be beyond the scope of this work; however, the issue may be taken up in a future study by using other climate models to calculate the climate indices, carry out the extrapolation of the climate forcings with these alternative indices and assess the impact on future ice-sheet evolution.

Furthermore, future work in the direction of long-term simulations of ice-sheet response to climate change should aim at employing more direct, rather than extrapolated, GCM projections beyond 2100 and involving an ensemble of ice-sheet models to allow an improved assessment of uncertainties. Within ISMIP6, this is currently planned within the ISMIP6 Projections 2300 Antarctica initiative for the AIS (<https://thehub.org/groups/ismip6/wiki/ISMIP6-Projections2300-Antarctica>, last access: 2023-05-11). In detail, this initiative focuses on projections extended until 2300 (as in the present study) based on CMIP5 and CMIP6 GCM outputs. Some experiments will use repeated climate forcing from the late 21st century, sampled randomly between 2100 and 2300 (similar to the approach by Chambers and others, 2022), while others will be based on output from GCMs directly run until 2300 under CMIP forcing pathways. We will contribute to these projections with the SICOPOLIS model.

Supplementary material. The supplementary material for this article can be found at <https://doi.org/10.1017/jog.2023.41>.

Code and data availability. SICOPOLIS (SICOPOLIS Authors, 2021) is free and open-source software, published on a persistent Git repository hosted by the Alfred Wegener Institute for Polar and Marine Research (AWI) in Bremerhaven, Germany (<https://gitlab.awi.de/sicopolis/sicopolis/>). The output data produced for this study are available at Zenodo, <https://doi.org/10.5281/zenodo.7773727>.

Acknowledgements. We thank the Scientific Editor Frank Pattyn and two reviewers for constructive remarks and suggestions that helped to improve the manuscript. We thank Jorge Bernales (Utrecht University) and Reinhard Calov (PIK Potsdam) for their recent contributions to the development of the SICOPOLIS model, and Tom Dangleterre (Hokkaido University) for post-processing our output data for the Zenodo archive. Some colour schemes of our figures were taken from Paul Tol's (SRON Netherlands Institute for Space Research) online resource at <https://personal.sron.nl/~paul> (last access:

2023-05-11). We thank the Climate and Cryosphere (CliC) effort, which provided support for ISMIP6 through sponsoring of workshops, hosting the ISMIP6 website and wiki and promoting ISMIP6. We acknowledge the World Climate Research Programme, which, through its Working Group on Coupled Modelling, coordinated and promoted CMIP5 and CMIP6. We thank the climate modelling groups for producing their model output and making it available; the Earth System Grid Federation (ESGF) for archiving the CMIP data and providing access to it; the University at Buffalo for ISMIP6 data distribution and upload; and the multiple funding agencies who support CMIP5, CMIP6 and ESGF. We thank the ISMIP6 steering committee, the ISMIP6 model selection group and ISMIP6 dataset preparation group for their continuous engagement in defining ISMIP6. This is ISMIP6 contribution No. 28.

Authors' contributions. Ralf Greve, Christopher Chambers and Ayako Abe-Ouchi designed the study. Takashi Obase, Fuyuki Saito, Wing-Le Chan and Ayako Abe-Ouchi ran the MIROC simulations. Ralf Greve, Christopher Chambers and Takashi Obase computed the climate indices and the extrapolated ISMIP6 climate forcing. Ralf Greve ran the SICOPOLIS simulations with support from Christopher Chambers. All authors discussed and interpreted the results. Ralf Greve wrote the manuscript with contributions from all authors.

Financial support. Ralf Greve, Christopher Chambers, Wing-Le Chan and Ayako Abe-Ouchi were supported by Japan Society for the Promotion of Science (JSPS) KAKENHI Grant No. JP17H06323. Ralf Greve, Wing-Le Chan and Ayako Abe-Ouchi were supported by JSPS KAKENHI Grant No. JP17H06104. Takashi Obase, Fuyuki Saito and Ayako Abe-Ouchi were supported by JSPS Grant-in-Aid for Japan–France Integrated Action Program (SAKURA Program) No. JPJSBP120213203.

References

- Abe-Ouchi A and 6 others** (2013) Insolation-driven 100,000-year glacial cycles and hysteresis of ice-sheet volume. *Nature* **500**(7461), 190–193. doi:[10.1038/nature12374](https://doi.org/10.1038/nature12374)
- Alley RB and 7 others** (2015) Oceanic forcing of ice-sheet retreat: West Antarctica and more. *Annual Review of Earth and Planetary Sciences* **43** (1), 207–231. doi:[10.1146/annurev-earth-060614-105344](https://doi.org/10.1146/annurev-earth-060614-105344)
- Bakker P and 17 others** (2016) Fate of the Atlantic meridional overturning circulation: strong decline under continued warming and Greenland melting. *Geophysical Research Letters* **43**, 12252–12260. doi:[10.1002/2016GL070457](https://doi.org/10.1002/2016GL070457)
- Barthel A and 9 others** (2020) CMIP5 model selection for ISMIP6 ice sheet model forcing: Greenland and Antarctica. *The Cryosphere* **14**(3), 855–879. doi:[10.5194/tc-14-855-2020](https://doi.org/10.5194/tc-14-855-2020)
- Bernales J, Rogozhina I, Greve R and Thomas M** (2017) Comparison of hybrid schemes for the combination of shallow approximations in numerical simulations of the Antarctic ice sheet. *The Cryosphere* **11**(1), 247–265. doi:[10.5194/tc-11-247-2017](https://doi.org/10.5194/tc-11-247-2017)
- Blatter H and Greve R** (2015) Comparison and verification of enthalpy schemes for polythermal glaciers and ice sheets with a one-dimensional model. *Polar Science* **9**(2), 196–207. doi:[10.1016/j.polar.2015.04.001](https://doi.org/10.1016/j.polar.2015.04.001)
- Bulthuis K, Arnst M, Sun S and Pattyn F** (2019) Uncertainty quantification of the multi-centennial response of the Antarctic ice sheet to climate change. *The Cryosphere* **13**(4), 1349–1380. doi:[10.5194/tc-13-1349-2019](https://doi.org/10.5194/tc-13-1349-2019)
- Calov R and 8 others** (2018) Simulation of the future sea level contribution of Greenland with a new glacial system model. *The Cryosphere* **12**(10), 3097–3121. doi:[10.5194/tc-12-3097-2018](https://doi.org/10.5194/tc-12-3097-2018)
- Chambers C, Greve R, Obase T, Saito F and Abe-Ouchi A** (2022) Mass loss of the Antarctic ice sheet until the year 3000 under a sustained late-21st-century climate. *Journal of Glaciology* **68**(269), 605–617. doi:[10.1017/jog.2021.124](https://doi.org/10.1017/jog.2021.124)
- DeConto RM and 12 others** (2021) The Paris climate agreement and future sea-level rise from Antarctica. *Nature* **593**(7857), 83–89. doi:[10.1038/s41586-021-03427-0](https://doi.org/10.1038/s41586-021-03427-0)
- Dutton A and 8 others** (2015) Sea-level rise due to polar ice-sheet mass loss during past warm periods. *Science* **349**(6244), aaa4019. doi:[10.1126/science.aaa4019](https://doi.org/10.1126/science.aaa4019)
- Edwards TL and 83 others** (2021) Projected land ice contributions to twenty-first-century sea level rise. *Nature* **593**(7857), 74–82. doi:[10.1038/s41586-021-03302-y](https://doi.org/10.1038/s41586-021-03302-y)
- Eyring V and 6 others** (2016) Overview of the coupled model intercomparison project Phase 6 (CMIP6) experimental design and organization. *Geoscientific Model Development* **9**(5), 1937–1958. doi:[10.5194/gmd-9-1937-2016](https://doi.org/10.5194/gmd-9-1937-2016)
- Fortuin JPF and Oerlemans J** (1990) Parameterization of the annual surface temperature and mass balance of Antarctica. *Annals of Glaciology* **14**, 78–84. doi:[10.3189/S0260305500008302](https://doi.org/10.3189/S0260305500008302)
- Franco B, Fettweis X, Lang C and Ericpicum M** (2012) Impact of spatial resolution on the modelling of the Greenland ice sheet surface mass balance between 1990–2010, using the regional climate model MAR. *The Cryosphere* **6**(3), 695–711. doi:[10.5194/tc-6-695-2012](https://doi.org/10.5194/tc-6-695-2012)
- Garbe J, Albrecht T, Levermann A, Donges JF and Winkelmann R** (2020) The hysteresis of the Antarctic ice sheet. *Nature* **585**(7826), 538–544. doi:[10.1038/s41586-020-2727-5](https://doi.org/10.1038/s41586-020-2727-5)
- Gasson E, DeConto RM, Pollard D and Levy RH** (2016) Dynamic Antarctic ice sheet during the early to mid-Miocene. *Proceedings of the National Academy of Sciences of the United States of America* **113**(13), 3459–3464. doi:[10.1073/pnas.1516130113](https://doi.org/10.1073/pnas.1516130113)
- Gladstone RM and 5 others** (2017) Marine ice sheet model performance depends on basal sliding physics and sub-shelf melting. *The Cryosphere* **11**(1), 319–329. doi:[10.5194/tc-11-319-2017](https://doi.org/10.5194/tc-11-319-2017)
- Goelzer H and 41 others** (2020) The future sea-level contribution of the Greenland ice sheet: a multi-model ensemble study of ISMIP6. *The Cryosphere* **14**(9), 3071–3096. doi:[10.5194/tc-14-3071-2020](https://doi.org/10.5194/tc-14-3071-2020)
- Golledge NR and 5 others** (2015) The multi-millennial Antarctic commitment to future sea-level rise. *Nature* **526**(7573), 421–425. doi:[10.1038/nature15706](https://doi.org/10.1038/nature15706)
- Greve R and 5 others** (2020a) ISMIP6 future projections for the Antarctic ice sheet with the model SICOPOLIS. Technical report, Zenodo. doi:[10.5281/zenodo.3971232](https://doi.org/10.5281/zenodo.3971232)
- Greve R and Blatter H** (2016) Comparison of thermodynamics solvers in the polythermal ice sheet model SICOPOLIS. *Polar Science* **10**(1), 11–23. doi:[10.1016/j.polar.2015.12.004](https://doi.org/10.1016/j.polar.2015.12.004)
- Greve R and Chambers C** (2022) Mass loss of the Greenland ice sheet until the year 3000 under a sustained late-21st-century climate. *Journal of Glaciology* **68**(269), 618–624. doi:[10.1017/jog.2022.9](https://doi.org/10.1017/jog.2022.9)
- Greve R, Chambers C and Calov R** (2020b) ISMIP6 future projections for the Greenland ice sheet with the model SICOPOLIS. Technical report, Zenodo. doi:[10.5281/zenodo.3971251](https://doi.org/10.5281/zenodo.3971251)
- Gudmundsson GH, Paolo FS, Adusumilli S and Fricker HA** (2019) Instantaneous Antarctic ice sheet mass loss driven by thinning ice shelves. *Geophysical Research Letters* **46**(23), 13903–13909. doi:[10.1029/2019GL085027](https://doi.org/10.1029/2019GL085027)
- Haseloff M and Sergienko OV** (2018) The effect of buttressing on grounding line dynamics. *Journal of Glaciology* **64**(245), 417–431. doi:[10.1017/jog.2018.30](https://doi.org/10.1017/jog.2018.30)
- The IMBIE Team** (2018) Mass balance of the Antarctic ice sheet from 1992 to 2017. *Nature* **558**(7709), 219–222. doi:[10.1038/s41586-018-0179-y](https://doi.org/10.1038/s41586-018-0179-y)
- The IMBIE Team** (2020) Mass balance of the Greenland Ice Sheet from 1992 to 2018. *Nature* **579**(7798), 233–239. doi:[10.1038/s41586-019-1855-2](https://doi.org/10.1038/s41586-019-1855-2)
- IPCC** (2021) *Climate Change 2021: The Physical Science Basis. Contribution of Working Group I to the Sixth Assessment Report of the Intergovernmental Panel on Climate Change*. Cambridge, UK, New York, NY, USA: Cambridge University Press. URL: <https://www.ipcc.ch/report/ar6/wg1/>.
- Joughin I, Smith BE and Medley B** (2014) Marine ice sheet collapse potentially under way for the Thwaites Glacier Basin, West Antarctica. *Science* **344**(6185), 735–738. doi:[10.1126/science.1249055](https://doi.org/10.1126/science.1249055)
- Jourdain NC and 6 others** (2020) A protocol for calculating basal melt rates in the ISMIP6 Antarctic ice sheet projections. *The Cryosphere* **14**(9), 3111–3134. doi:[10.5194/tc-14-3111-2020](https://doi.org/10.5194/tc-14-3111-2020)
- Levermann A and 6 others** (2013) The multimillennial sea-level commitment of global warming. *Proceedings of the National Academy of Sciences of the United States of America* **110**(34), 13745–13750. doi:[10.1073/pnas.1219414110](https://doi.org/10.1073/pnas.1219414110)
- Lipscomb WH and 5 others** (2021) ISMIP6-based projections of ocean-forced Antarctic ice sheet evolution using the community ice sheet model. *The Cryosphere* **15**(2), 633–661. doi:[10.5194/tc-15-633-2021](https://doi.org/10.5194/tc-15-633-2021)
- Lowry DP, Krapp M, Golledge NR and Alevopoulos-Borrill A** (2021) The influence of emissions scenarios on future Antarctic ice loss is unlikely to emerge this century. *Communications Earth & Environment* **2**, 221. doi:[10.1038/s43247-021-00289-2](https://doi.org/10.1038/s43247-021-00289-2)

- Meinshausen M and 12 others** (2011) The RCP greenhouse gas concentrations and their extensions from 1765 to 2300. *Climatic Change* **109**(1-2), 213–241. doi:[10.1007/s10584-011-0156-z](https://doi.org/10.1007/s10584-011-0156-z)
- Mercer JH** (1978) West Antarctic ice sheet and CO₂ greenhouse effect: a threat of disaster. *Nature* **271**(5643), 321–325. doi:[10.1038/271321a0](https://doi.org/10.1038/271321a0)
- Morlighem M and 31 others** (2017) BedMachine v3: Complete bed topography and ocean bathymetry mapping of Greenland from multibeam echo sounding combined with mass conservation. *Geophysical Research Letters* **44**(21), 11051–11061. doi:[10.1002/2017GL074954](https://doi.org/10.1002/2017GL074954)
- Morlighem M and 36 others** (2020) Deep glacial troughs and stabilizing ridges unveiled beneath the margins of the Antarctic ice sheet. *Nature Geoscience* **13**(2), 132–137. doi:[10.1038/s41561-019-0510-8](https://doi.org/10.1038/s41561-019-0510-8)
- Nowicki SMJ and 8 others** (2016) Ice sheet model intercomparison project (ISMIP6) contribution to CMIP6. *Geoscientific Model Development* **9**(12), 4521–4545. doi:[10.5194/gmd-9-4521-2016](https://doi.org/10.5194/gmd-9-4521-2016)
- Nowicki S and 29 others** (2020) Experimental protocol for sea level projections from ISMIP6 stand-alone ice sheet models. *The Cryosphere* **14**(7), 2331–2368. doi:[10.5194/tc-14-2331-2020](https://doi.org/10.5194/tc-14-2331-2020)
- Payne AJ and 63 others** (2021) Future sea level change under Coupled Model Intercomparison Project Phase 5 and Phase 6 scenarios from the Greenland and Antarctic ice sheets. *Geophysical Research Letters* **48**(16), e2020GL091741. doi:[10.1029/2020GL091741](https://doi.org/10.1029/2020GL091741)
- Pollard D and DeConto RM** (2009) Modelling West Antarctic ice sheet growth and collapse through the past five million years. *Nature* **458**(7236), 329–332. doi:[10.1038/nature07809](https://doi.org/10.1038/nature07809)
- Rignot E, Mouginot J, Morlighem M, Seroussi H and Scheuchl B** (2014) Widespread, rapid grounding line retreat of Pine Island, Thwaites, Smith, and Kohler glaciers, West Antarctica, from 1992 to 2011. *Geophysical Research Letters* **41**(10), 3502–3509. doi:[10.1002/2014GL060140](https://doi.org/10.1002/2014GL060140)
- Schaeffer M, Hare W, Rahmstorf S and Vermeer M** (2012) Long-term sea-level rise implied by 1.5°C and 2°C warming levels. *Nature Climate Change* **2**(12), 867–870. doi:[10.1038/nclimate1584](https://doi.org/10.1038/nclimate1584)
- Schoof C** (2007) Ice sheet grounding line dynamics: Steady states, stability, and hysteresis. *Journal of Geophysical Research: Earth Surface* **112**(F3), F03S28. doi:[10.1029/2006JF000664](https://doi.org/10.1029/2006JF000664)
- Seroussi H and 46 others** (2020) ISMIP6 Antarctica: a multi-model ensemble of the Antarctic ice sheet evolution over the 21st century. *The Cryosphere* **14**(9), 3033–3070. doi:[10.5194/tc-14-3033-2020](https://doi.org/10.5194/tc-14-3033-2020)
- SICOPOLIS Authors** (2021) SICOPOLIS (version 5-dev, branch develop, commit hash cb5a75b92). GitLab, Alfred Wegener Institute for Polar and Marine Research, Bremerhaven, Germany, URL <https://gitlab.awi.de/sicopolis/sicopolis>.
- Sun S and 28 others** (2020) Antarctic ice sheet response to sudden and sustained ice-shelf collapse (ABUMIP). *Journal of Glaciology* **66**(260), 891–904. doi:[10.1017/jog.2020.67](https://doi.org/10.1017/jog.2020.67)
- Thomas RH and Bentley CR** (1978) A model for Holocene retreat of the West Antarctic ice sheet. *Quaternary Research* **10**(2), 150–170. doi:[10.1016/0033-5894\(78\)90098-4](https://doi.org/10.1016/0033-5894(78)90098-4)
- Trusel LD and 6 others** (2015) Divergent trajectories of Antarctic surface melt under two twenty-first-century climate scenarios. *Nature Geoscience* **8**(12), 927–932. doi:[10.1038/ngeo2563](https://doi.org/10.1038/ngeo2563)
- Turney CSM and 31 others** (2020) Early Last Interglacial ocean warming drove substantial ice mass loss from Antarctica. *Proceedings of the National Academy of Sciences of the United States of America* **117**(8), 3996–4006. doi:[10.1073/pnas.1902469117](https://doi.org/10.1073/pnas.1902469117)
- Van Breedam J, Goelzer H and Huybrechts P** (2020) Semi-equilibrated global sea-level change projections for the next 10 000 years. *Earth System Dynamics* **11**(4), 953–976. doi:[10.5194/esd-11-953-2020](https://doi.org/10.5194/esd-11-953-2020)
- Weertman J** (1974) Stability of the junction of an ice sheet and an ice shelf. *Journal of Glaciology* **13**(67), 3–11. doi:[10.3189/S0022143000023327](https://doi.org/10.3189/S0022143000023327)